Published on 15 January 2024. Downloaded by Beijing Institute of Nanoenergy and Nanosystems CAS on 1/22/2024 11:26:07 AM.

Journal of Materials Chemistry B

ROYAL SOCIETY OF CHEMISTRY

PAPER

View Article Online
View Journal

Check for updates

Cite this: DOI: 10.1039/d3tb02466k

A light-sensitive protein-based wearable pH biometer†

Wenxue Li,[ab] Siyuan Chen,[c] Shiwang Xie,[b] Xianmao Lu,[ab] Zhou Li,*[b] Yujia Lv*[b] and Dan Luo*[b]

Received 20th October 2023,
Accepted 22nd December 2023

DOI: 10.1039/d3tb02466k

rsc.li/materials-b

Bacteriorhodopsin is a biological material with excellent photosensitivity properties. It can directly convert optical signals into electrical signals and is widely used in various biosensors. Here, we present a bR-based wearable pH biometer that can be used to monitor wound infection. The mechanism of the pH-sensitive effect of the bR electrode is explained, which generates a transient photovoltage under light irradiation and a negative photovoltage when the lamp is turned off. Since the photoelectric signal of bR is affected by different pH values, the photovoltage is changed by adjusting the pH value. The ratio (V_n/V_p) of negative photovoltage (V_n) to positive photovoltage (V_p) has a good linear relationship (R^2 = 0.9911) in the pH range of 4.0–10.0. *In vitro* experiments using rats as a model confirmed that this wearable pH biometer can monitor pH changes that occur in wound infection.

Introduction

Infection is a complication of chronic and polar wounds that delays the healing process, and the cessation or slowing of wound healing greatly increases bacterial colonization.[1,2] In aggravated circumstances, it may even lead to a list of complications, for instance, sepsis and tissue injuries, which can negatively impact the quality of the patient's life and can be a heavy burden on the patient's own finances and healthcare systems.[3] Therefore, opportune observation and therapeutics of infection are very significant for patients with traumatic injuries and surgical wounds that have not healed.[4] Previous studies have shown that the pH range of the healthy body skin surface is between 4.0 and 6.0, while the pH of the area of trauma reaches above 8.0, resulting from the release of bacterial metabolites into the wound environment.[5] Therefore, the pH of the wound is the main physiological parameter for studying the wound state.

The change of the pH value is a key indicator in wound repair, drug research, and medical diagnosis, and pH detection is crucial in the research process and practical application in various disciplines.[6–8] With the research and development of flexible electronic products, wearable medical devices applied to monitor physiological parameters have attracted great attention. For example, colorimetric detection of the pH of wound liquid relies on the sensitivity of the dye to different pH values and changes in the color of the pH indicator can be investigated with the unaided eye in the pH range of wound infection.[9–11] However, the detection sensitivity of colorimetric pH sensors is not high enough and the detection results are prone to false alarms.[12] In addition, different nanomaterials can be combined with electronic devices to form wearable sensors consisting of pH-sensitive working electrodes and reference electrodes, which can identify unhealed or infected wounds at an early stage.[3,13,14] Since there are no relevant reports on the long-term biocompatibility and toxicity of nanomaterials, their use is still controversial.[15] Therefore, it is urgent to develop a stable and biocompatible pH sensor for monitoring wound pH. Recently, some biological materials have demonstrated strong ability to perceive acid–base solutions and can sensitively detect pH changes; there have been many studies on the preparation of pH sensors using biological materials, such as pH sensors using enhanced blue-green fluorescent proteins with a strong sensitivity to pH.[16] Protein and organic dye nanoions are combined into a hybrid system to monitor small pH changes.[17] A new biohybrid pH sensor was designed using the photosensitive protein proteorhodopsin.[18]

Bacteriorhodopsin (bR) is a typical proton pump based on light drive and has excellent photosensitivity properties.[19,20] Under photoexcitation, the directional transmission of protons occurs, generating electrical signals and realizing the optical energy can transform into electrical energy.[21] In this paper, we propose a flexible wearable pH biometer based on biological materials (Scheme 1), describe the preparation and characterization of the

[a] School of Chemistry and Chemical Engineering, Guangxi University, Nanning, 530004, China
[b] Beijing Institute of Nanoenergy and Nanosystems, Chinese Academy of Sciences, Beijing, 101400, China. E-mail: zli@binn.cas.cn, lizhou@binn.cas.cn, lvyujia@binn.cas.cn, luodan@binn.cas.cn
[c] Shanghai Pinghe School, Shanghai, 201203, China

† Electronic supplementary information (ESI) available. See DOI: https://doi.org/10.1039/d3tb02466k

Published on 15 January 2024. Downloaded by Beijing Institute of Nanoenergy and Nanosystems CAS on 1/22/2024 11:26:07 AM.

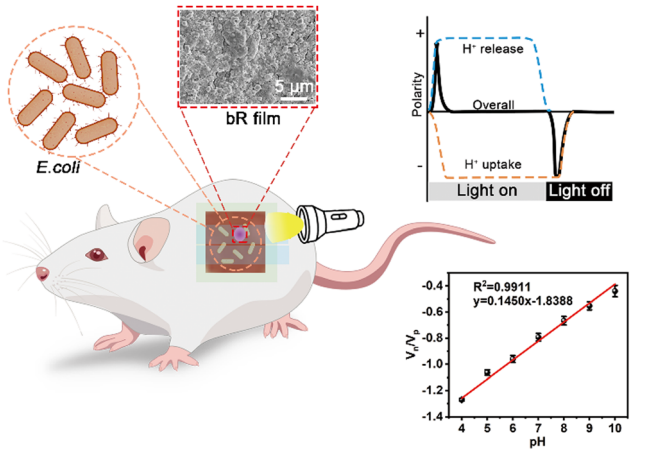

Scheme 1 Application and detection mechanism of bR monitoring of pH values of wound infection.

photosensitive protein bR photoelectrode, and measure it in the pH within the limits of 4.0–10.0, the photogenerated voltage response signal ((V_n/V_p), the ratio of negative photovoltage (V_n) to positive photovoltage (V_p)) has a nice linear relationship with pH (R^2 = 0.9911), and the experimental results are compared with traditional glass pH electrodes with high accuracy (R^2 = 0.9933) that verifies the ability of pH biometers to monitor pH in practical applications. *In vitro* experiments using a rat model of *Escherichia coli* (*E. coli*) infection confirm that pH changes could be detected in the early stages of infection.

Experimental section

Materials and reagents

NaCl, NaOH, KCl, Na_2HPO_4, HCl, and KH_2PO_4 were purchased from Aladdin. These chemical medicines used were of analytical grade and no further purification was performed in this study. The working solution (PBS) consists of phosphate and chloride, and the pH of the PBS buffer is adjusted by adding 1 M NaOH solution. Mixing different volumes of acidic PBS and alkaline PBS to change the pH required during the test.

Extraction and purification of bR protein

The bR protein was isolated and purified from Halobacterium strain R1M1 according to the standard operating procedure described by predecessors. The cells were collected by centrifugation at 13 000*g* for 15 min, the precipitate was retained, and the supernatant was removed. Then, deionized water was added for dialysis overnight to lyse the cells to obtain a red lysate. Next, the red lysate was centrifuged to remove the red supernatant (40 000*g* centrifuged for 40 min), and then, the red-purple precipitate was resuspended with deionized water, centrifuged under the same conditions, and repeated until the supernatant was almost colorless. The suspension was washed and precipitated 2–3 times in deionized water until the supernatant was colorless.[22]

Preparation of wearable pH biometers

Indium tin oxide (ITO) was ultrasonically cleaned sequentially in acetone, ethanol, and deionized water for 30 min. Then, 10 μL of bR was dropped onto the washed ITO film to form an oval ring with a radius of 2.5 mm. Due to the volatilization-induced assembly, the solvent was volatilized, and after 45 min of deposition at ~45 °C, a dense and uniform bR film formed on the surface of the ITO film. Finally, deionized washing was used to remove poorly deposited proteins from the film.

Characterization of bR electrodes

SU8020 cold field scanning electron microscopy was applied to characterize the surface topography and cross-section of the bR electrode. The morphological structure of the bR film on the positive light electrode was studied using atomic force microscopy (MFP-3D-SA). Confocal Raman microscopy (LabRAM HR Evolution) was used to record Raman spectroscopy of deposited bR films. The UV-vis absorption spectrum was measured using a PerkinElmer Lambda 35 UV/vis spectrophotometer.

Collection of the photoelectric signals

The open circuit voltage was tested using the Chi760e electrochemical workstation. A three-electrode artificial biophotoelectric system was used in all electrochemical tests, in which the bR/ITO electrodes are regarded as the working electrode, the ITO film as the counter electrode, and the reference electrode. The xenon lamp (CEL-HXF300) provides a continuous broadband light source with a luminous output of 200.0 mW cm^{-2}. The photovoltage was tested as a background source under dark adaptation conditions, and the light was manually chopped with 5 s as the time unit.

In vitro biocompatibility assessment

The biocompatibility of bR was investigated by testing the activity of L929 cells by CCK-8. Cells were cultured with DMEM-containing high sugar medium (Solarbio) in a humidified incubator (5% CO_2). All materials were cut into 4.5 mm square shapes, placed in fresh medium and incubated for 24 h. Cells were seeded into 96-well plates and incubated with extracts extracted once daily. The CCK-8 kit was used to assess cell viability according to the instructions.

Before the cytotoxicity tests, the bR was dispersed in the medium at a concentration of 50 ug ml^{-1}. After washing with PBS, trypsin digestion, centrifugation, DMEM resuspension and cell counting plate counting, L929 cells were sequentially seeded into 12-well plates and cultured at 37 °C with 5% CO_2 for 48 h. After treatment, the original medium was washed thoroughly with PBS and then stained with Calcein/PI Cell Viability and Cytotoxicity Assay Kit (C2015M) and observed and photographed under a fluorescence microscope.

Wound infection surveillance

All animal experiments were performed according to protocols approved by the Committee on Ethics of the Beijing Institute of Nanoenergy and Nanosystems (2023012LD). A rat model was

This journal is © The Royal Society of Chemistry 2024

Published on 15 January 2024. Downloaded by Beijing Institute of Nanoenergy and Nanosystems CAS on 1/22/2024 11:26:07 AM.

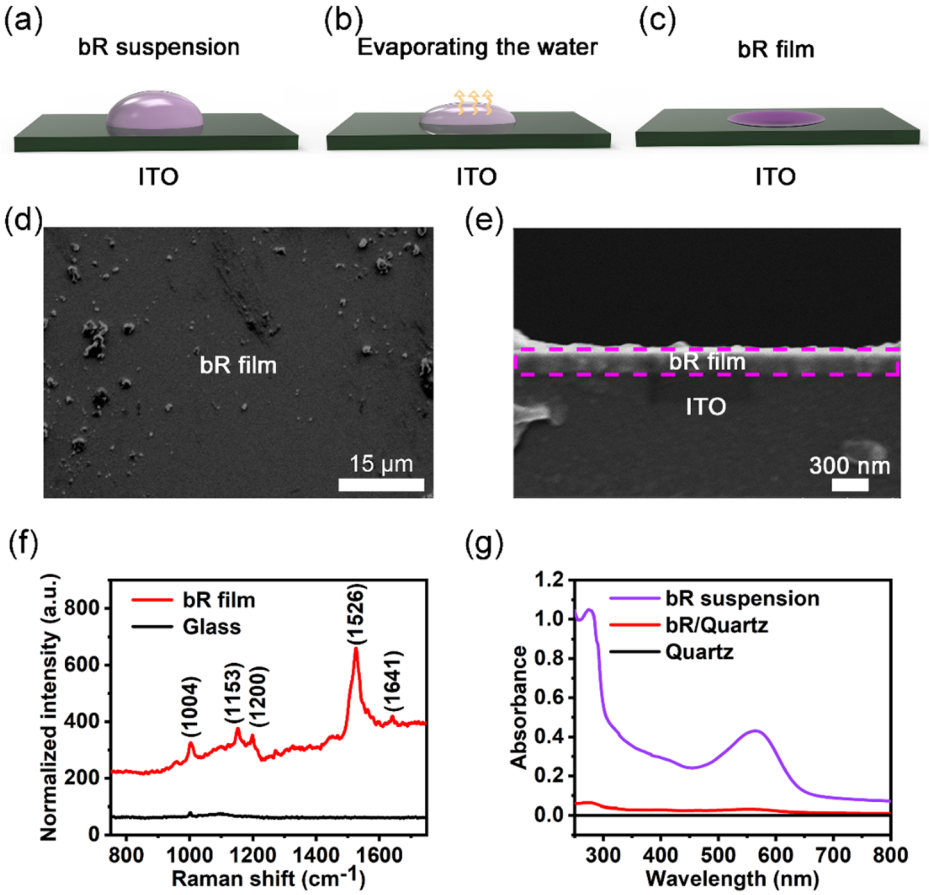

Fig. 1 Preparation of the bR photoelectrode and its various characterization methods. (a)–(c) Volatilization-induced assembly to prepare a bR based photoelectrode. (d) and (e) SEM image (surface chart and cross sectional graph) of the bR film overlaid on the ITO. (f) Raman spectra of bR membranes in the range of 750–1750 nm. (g) UV-vis absorption spectrum of the bR suspension and film in the range of 250–800 nm.

created to obtain a wound infection assessment by infecting a wound with *E. coli*. Two 6-week-old male Sprague-Dawley rats (SD rats) were used in the experiment, divided into uninfected and infected (purchased from Beijing Vital River Laboratory Animal Technology Co., Ltd). These SD rats were anesthetized using isoflurane anesthetic gas (anesthesia machine purchased from Yuyan Instrument). The hair on the back of the SD rat was then shaved off with a razor to expose the skin, disinfected with 75% alcohol, a square skin wound (approximately 2 cm × 2 cm) was cut on the rat's back with scissors, the wound was cleaned with 0.9% sterile saline, and then an *E. coli* suspension (500 μL, 1×10^9 CFU) was applied to the skin wound to induce bacterial infection. The experiment used normal saline as a control group. After wound treatment was complete, a flexible pH biometer was worn on the wound part to monitor the infection status of the wound.

Result and discussion

Preparation and characterization of bR photoelectrodes

In recent years, volatile-induced assembly has been widely applied in the assembly of non-volatile solutes, which has the characteristics of easy operation, low cost and strong applicability. The evaporation of the droplet suspension on the wettable surface can induce self-assembly, forming a one-dimensional ring deposit with a regular structure.[23] Therefore, we prepared a photoelectrode based on a biomaterial pH biometer by volatilization-induced assembly. As shown in the schematic diagram in Fig. 1(a–c), the bR suspension (Fig. S1, ESI†) was dropped onto the washed ITO film sheet to form a ring-shaped droplet and placed on a heater for evaporation induction. The bR film densely and uniformly formed on the ITO film surface as the water in the suspension evaporated. To explore whether the bR electrode still retains the characteristics of bR itself, we have characterized it using various methods. As shown in Fig. 1(d and e), scanning electron microscopy (SEM) was used to characterize the surface and cross-sectional topography of the film, determining that the ITO film is covered with a uniformly dense bR film with a basic thickness of 0.3 μm. Enlargement of the bR membrane reveals that many bR proteins are loaded (Fig. S2, ESI†). Atomic force microscopy (AFM) is used to observe the outside face structure of the bR film, and the three protrusions of the bR molecular trimer can be seen, indicating that it maintains its trimer structure. There is an obvious island structure in the bR film, the height of the

Published on 15 January 2024. Downloaded by Beijing Institute of Nanoenergy and Nanosystems CAS on 1/22/2024 11:26:07 AM.

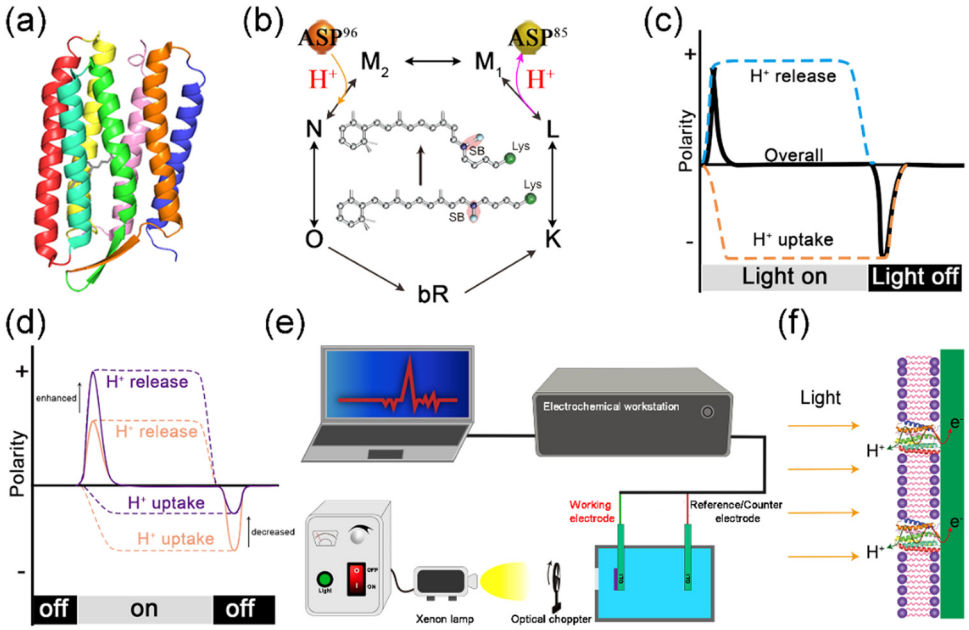

Fig. 2 Working mechanism of the pH biometer based on the photosensitive protein bR. (a) Protein structure diagrammatic drawing of the bR. (b) The photocycle process of bR: under light conditions, the retina passes through the ground state of bR → K ↔ L ↔ M ↔ N → O intermediates (illustration: transition diagram of the configuration of the retinal in the bR molecule under illumination). (c) and (d) Proton uptake and release model of the bR protein in the light–dark adaptation state under alkaline conditions. (e) Schematic diagram of the photovoltage test system. (f) Schematic of proton transfer of the bR protein immobilized on ITO.

"island" protrusion is about ~15 nm. It was further confirmed that the bR film covered with the ITO film still maintained a good structural form (Fig. S3, ESI†).

To further demonstrate the deposition of bR on the electrode, a Raman test was performed (Fig. 1(f)). Since ITO films absorb in the UV region, glass slides were chosen instead of ITO films to prepare samples. It can be seen that the membrane contains three main characteristic peaks: an alkenyl C=C at 1526 cm^{-1}, a fingerprint C–C stretched bimodal of 1153 and 1200 cm^{-1}, and a methyl peak at 1004 cm^{-1}, indicating a typical bR Raman band. From this, it can be concluded that the bR film can be well covered on the photoelectrode. To verify that bR films deposited on ITO are sensitive to light, bR suspensions and bR films were characterized by UV-vis spectroscopy. Fig. 1(g) and Fig. S4 (ESI†) show that bR, whether in suspension or bR deposited on quartz glass, has characteristic peaks of bR at wavelengths of 280 nm and 568 nm, and the ratio of bR suspension A_{280} to A_{568} is 2.42. It shows that the bR photoelectrode prepared by volatilization-induced assembly still has its own unique optical properties. Moreover, according to Supplementary Note 1 (ESI†), the concentration of the bR suspension is known to be 0.99 mg mL^{-1}. These results show that bR still maintains a complete structure after film formation and still has good optical properties.

The mechanism of a bR-based pH biometer

The photosensitive protein bR molecule is a polypeptide chain composed of 248 amino acid residues, forming seven α transmembrane spiral beams on the inside of the lipid membrane. The molecule also contains the chromophore-retinal and is linked to Lysine-216 *via* the Schiff base.[24,25] There are two isomers (all-*trans* and 13-*cis*) in the retinal molecule, the retina in the darkness adaptation condition is all-*trans*, and the retina molecule isomeric changes from the all-*trans* configuration to the 13-*cis* configuration under light irradiation.[26,27] Under alkaline conditions, bR undergoes a photoperiod after being excited by light, as follows: bR → K ↔ L ↔ M ↔ N ↔ O → bR. In the process of transitioning from the L status to the M status, due to the action of coupling, Schiff base deprotonation releases protons to Asp-85 protons into Asp-85-H, and protons are also transmitted to the outside of the cell membrane, resulting in a greatly reduced pK_a of the proton release group (pK_a = 13.3 to pK_a = 2.2).[28] When transitioning from the M state to the N state, Asp-96-H is deprotonated to Asp-96, and the protons are transferred to the Schiff base and protonated again. Upon transition from the N state to the O state, Asp-96 re-protonation re-absorbs protons from within the cell, Asp-85-H re-deprotonation delivers protons to the proton release group, finally, bR returns to its original condition (Fig. 2(a and b)).[29,30] Therefore, the photo-charge movement generated by the bR electrode after being illuminated is shown in Fig. 2(c and d), with darkness as the background source, the proton pump starts when the light is instantaneous, the rapid occurrence of the retinal from total transfer to 13 *cis*, and the rapid polarization of the electron cloud in retinal causes charge separation. Under alkaline conditions, protons are transferred from the Schiff base to the proton acceptor Asp85 (the proton release group is pumped out of the cell) faster than the proton donor Asp96 to transfer a proton to the Schiff base (Asp96 inhales a proton from outside the cell), so the result is that protons are

 This journal is © The Royal Society of Chemistry 2024

Published on 15 January 2024. Downloaded by Beijing Institute of Nanoenergy and Nanosystems CAS on 1/22/2024 11:26:07 AM.

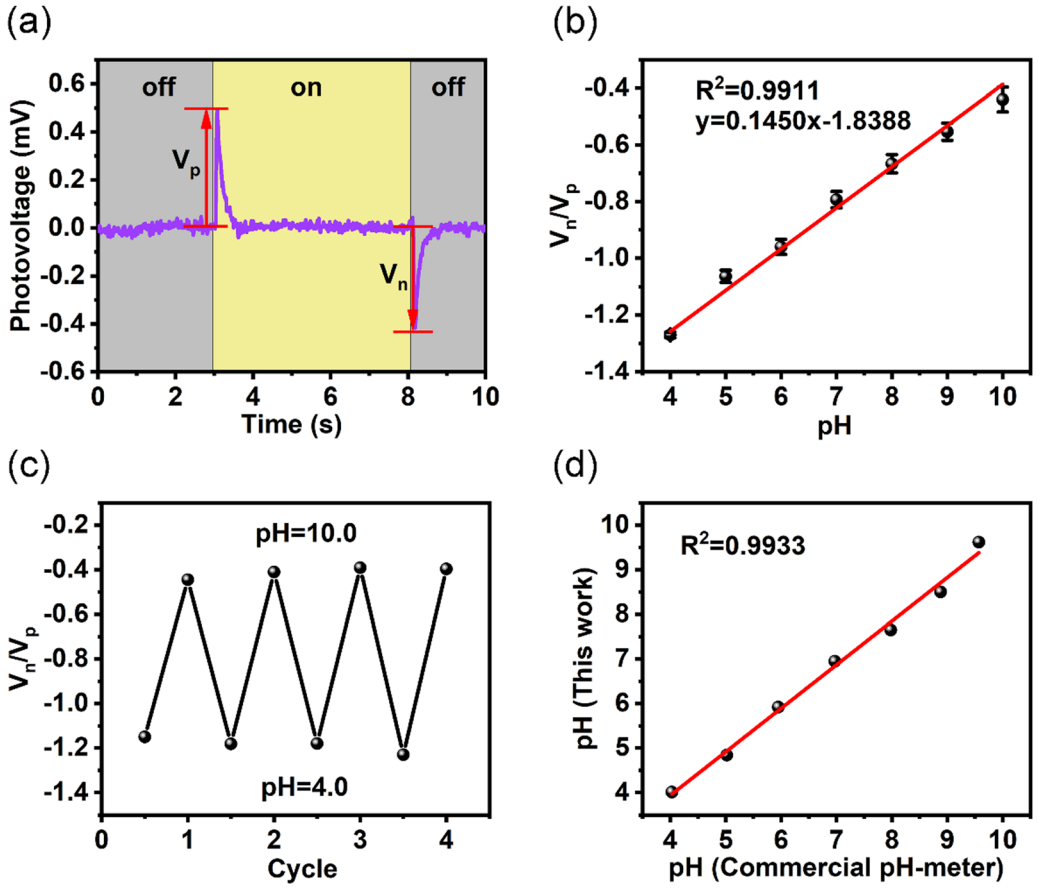

Fig. 3 The performance of the bR photoprotein-based pH biometer depends on the pH value. (a) Proton polarization-induced photovoltage transition plot in bR photosensitive proteins. (b) Photovoltage and dark voltage at diverse pH values (n = 3). (c) pH the reversibility of the bR photoelectrode (pH range 4.0–10.0, 5 s is a chopping time unit, light intensity is 200 mW cm^{-2}). (d) Correlation curve between the pH of a photosensitive protein bR-based pH biometer and the pH of a commercial pH meter.

pumped from intracellular to extracellular. The flexible bR photoelectrode was placed in a device for photoelectric testing, and a schematic of the photoelectric test system is shown in Fig. 2(e). The counter/reference electrode uses an ITO film (the resistance of the ITO film electrode is about 10 Ω), a xenon lamp as the power supply, and the baffle modulates the light and dark conditions. When the bR photoelectrode causes charge movement, the generated photovoltage signal is collected by electrochemical station testing (Fig. 2(f)).

Photovoltage response based on a bR photoelectrode pH biometer

It was found that positive signal peaks occur under photo adaptive conditions and negative signal peaks occur under dark-adaptive conditions. During photo cycling, the isomerization of the chromophore-retina inside bR produces charge transfer, resulting in potential differences. The velocity constants of proton release and uptake on the membrane surface depend primarily on pH.[31] When the bR electrode is irradiated with light, the pH in the solution affects a series of deprotonation and re-protonation processes of Schiff bases and their surrounding amino acids, altering the normal interaction between them and thus changing the production of photovoltage. As Nagel *et al.* explained, re-protonation of M1 occurs *via* Asp-85 and intensively relies on extracellular pH.[32,33] Therefore, the bR electrode is electrochemically tested, and the characteristics of the photoelectric characteristics are shown in Fig. 3(a). When illuminated, a positive photoelectric response signal V_p is rapidly formed. When the dark adaptation state is switched, the *cis*- and *trans* balance of the retina moves in the dominant direction of the all-*trans* configuration, and the continuous transmembrane conduction current generated by the proton pump couples with the coupling characteristics of the measurement circuit to form a potential difference,[34] forming a negative signal peak labeled V_n. Therefore, based on this property, electrochemical analysis was performed using a biohybridization device to test the performance of a pH biometer based on a photosensitive protein electrode. At different pH values, by inducing the light and dark voltage inversion of the bR electrode, it can be seen that V_n/V_p has an excellent linear relationship (R^2 = 0.9911, n = 7) with the pH in the range of 4.0–10.0, and eqn (1) establishes the quantitative relationship between V_n/V_p and pH (Fig. 3(b and c)).

$$y = 0.1450x - 1.8388 \quad (1)$$

Published on 15 January 2024. Downloaded by Beijing Institute of Nanoenergy and Nanosystems CAS on 1/22/2024 11:26:07 AM.

Table 1 pH sensors based on biomaterials

Materials	Method	pH range	R^2	n	F	$F_{0.01}(1, n-2)$	Ref.
QD@*B. subtilis* spore nanocomposites	Fluorescence	5.0–10.0	0.9946	6	736.741	21.198	36
Chitosan	Fluorescence	5.0–9.0	0.9906	11	948.447	10.561	37
Cellulose membrane	Fluorescence	1.0–7.0	0.9871	7	382.597	16.528	38
Hydrogel	Fluorescence	5.5–8.0	0.9950	10	1592.000	11.259	39
Bacterial cellulose/carboxymethyl cellulose	Colorimetry	4.0–9.0	0.9617	10	200.877	11.259	40
Bacteriorhodopsin	Electrochemistry	4.0–10.0	0.9911	7	556.780	16.258	This work

We also used commercially available pH meters to compare with pH biometers, and Fig. 3(d) clearly shows excellent correlation, which proves that flexible pH biometers based on bR electrodes have good utility and authenticity. Thus, we demonstrate that a photosensitive protein-based pH biometer can detect the pH of a solution.

Linear regression is usually used to identify the quantitative relationships between different variables in a set of data and is a statistical analysis method for studying the correlation between variables.[35] The independent and dependent variables can be derived from each other based on the established quantitative relationship. Not only that, but the regression equation also obtained can be verified by the method of statistical testing, and whether it can reflect the actual situation and have practical value according to the significance level (α). α is related to the sample size (n) and the correlation coefficient (R^2). Given an α, the corresponding $F_\alpha(1, n-2)$ value is obtained. In general, the quantitative relationship test, α will take 0.05 or 0.01, $1-\alpha$ indicates the reliability of the test. When $F < F_{0.05}(1, n-2)$, it means that x and y have no obvious linear relationship, which means that the regression equation cannot be trusted. When $F_{0.01}(1, n-2) \geq F \geq F_{0.05}(1, n-2)$, there is a noticeable linear relationship between x and y, while $F > F_{0.01}(1, n-2)$ x and y will present a significant correlation.

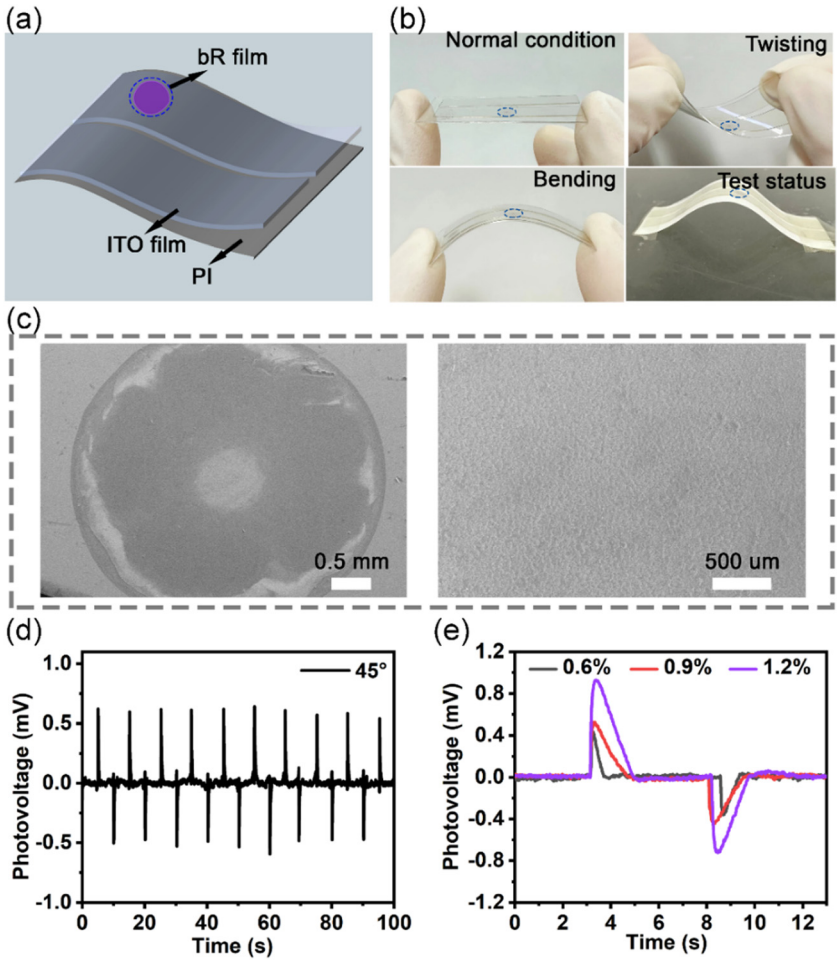

Fig. 4 Testing and characterization of flexible pH biometers. (a) Schematic diagram of a flexible pH biometer. (b) Various mechanical deformations of flexible pH biometers, including twisting and bending. (c) SEM diagram of the bR membrane after bending of the pH biometer. (d) Light and dark voltage test when bending (pH = 7.0). (e) Light and dark voltage tests with different salt content at pH 7.0.

This journal is © The Royal Society of Chemistry 2024

Published on 15 January 2024. Downloaded by Beijing Institute of Nanoenergy and Nanosystems CAS on 1/22/2024 11:26:07 AM.

Considering that electrolyte, light intensity and other factors affect the photoexcitation voltage of the bR electrode, we select the significance level $\alpha = 0.01$ to test eqn (1) and calculate the value of F as 556.780. Referring to other biomaterial-based pH sensors, in accordance with the data presented in Table 1, the relationship between the photosensitive protein bR electrode is very significant (the specific calculation process of the F value is based on Supplementary Note 2, ESI†).

Flexible and salt content testing of pH biometers

The softness of the material and the adhesivity to the laceration are significant for wearable sensors. We prepared a pH biometer using flexible materials with flexible ITO as the electrode and PI as the substrate (Fig. 4(a)). As a result, the device can undergo a variety of mechanical deformations, including bending and twisting, as shown in Fig. 4(b). It can be seen from Fig. 4(c and d) that the bR membrane on the curved pH biometer also covers the ITO electrode well without traces or cracks. After 100 seconds of testing, its electrochemical signal was also relatively stable, and the final pH was about 7.0. We also tested the effect of different salt solutions on pH and found that although the light and dark voltage increased with the increase in salt content, the final V_n/V_p was about 7.0 (Fig. 4(e), Fig. S5, ESI†). Therefore, the salt content has little effect on the pH of this pH biometer test. The effect of the chemical composition of other PBS on the pH tested by the wearable pH biometer was also studied (Fig. S6, ESI†), and it can be seen that although the different chemical compositions have an effect on the photovoltage of the device, they have little effect on the V_n/V_p ratio, and the calculated pH value is not much different from that of commercial pH meters. Additionally, we investigated the effect of temperature on the wearable pH biometer (Fig. S7, ESI†) and the increase in the output of the device as temperature increased (pH = 7.0). However, we brought the V_n/V_p obtained under high and low temperature conditions into the formula ($y = 0.1450x - 1.8388$) and found that the calculated pH value was approximate. Not only that, but we also performed tests at different optical densities, and the results in Fig. S8 (ESI†) show that the light–dark voltage increases with increasing optical density, but the calculated pH value is close to the result obtained with a pH meter (pH is approximately equal to 7). In the experiment, our only optical density condition was determined to be 200 mW cm^{-2}. We also tested the stability of the pH sensor (Fig. S9, ESI†), which was shown to have a fast response and good stability in an electrolyte at pH 7.0 for 1000 s under 1 Hz chopper light irradiation.

Skin wound infection monitoring with pH biometers

To ensure that the bR does not cause harm to wounds and tissues when touching the skin incision, progressive biocompatibility testing of the pH biometer and material is essential. The toxicity of wearable pH biometers and bR materials was assessed by the viability of L929 cells. The results of CCK-8 quantitative determination and calcein/PI fluorogram showed

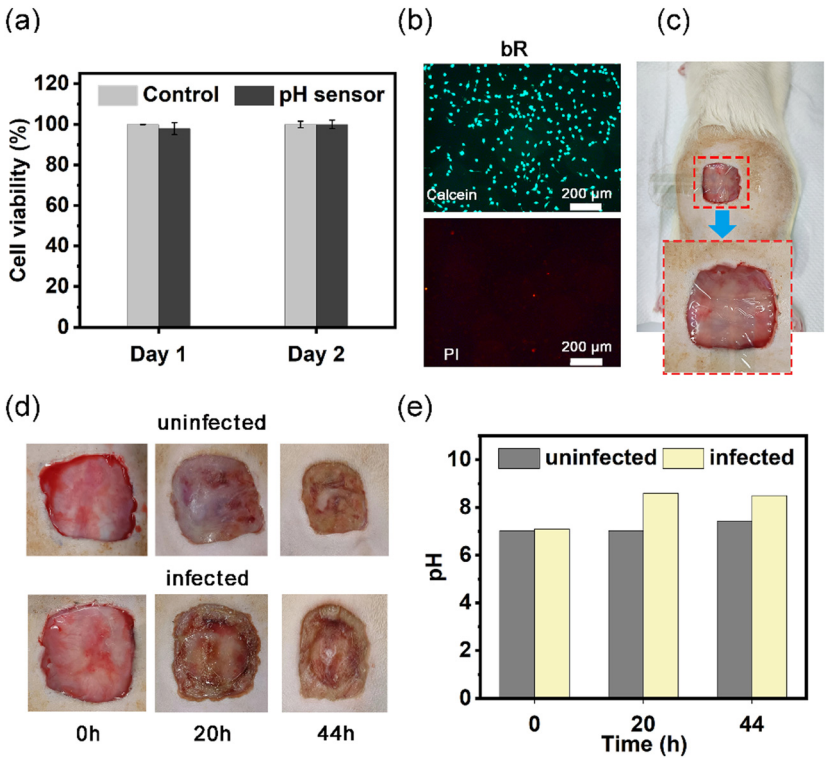

Fig. 5 Biocompatibility of sensors and surveillance of trauma infection. (a) Cell viability test of pH biometer materials. (b) Live/dead fluorescence image of bR after two days. (c) Picture of wounds in *E. coli* infected rats: uninfected and infected. (d) Physical image and sensor schematic of pH biometer wound monitoring. (e) Changes of pH in the wound.

Published on 15 January 2024. Downloaded by Beijing Institute of Nanoenergy and Nanosystems CAS on 1/22/2024 11:26:07 AM.

that the cells were relatively viable after two days with little change. The flexible pH biometer and the bR material are shown to be non-cytotoxic and biocompatible (Fig. 5(a) and (b)). In addition, we also tested the biocompatibility of the bR suspension (Fig. S10, ESI†), and showed that the relative cell activity of the bR suspension after diluting 50 times can still reach about 95% after three days. *E. coli* (Fig. S11, ESI†) is one of the most usual pathogens in wound infection, so inoculation of *E. coli* into wounds is used to establish a rat model of wound infection.[41,42] Fig. 5(c) shows a schematic representation of the flexible pH biometer and the wound connection image, showing that the device fits well with the wound. Animal wounds are shown in Fig. S12 (ESI†). (For the sensor to better fit the wound, a medical PU membrane with better flexibility than PI was selected when monitoring the pH value of wound infection in rats.) Even if the finger joint is bent at 45° and 105°, it also fits well on the finger (Fig. S13, ESI†). Photos of wounds in uninfected rats and infected rats at 0, 22, and 44 hours are shown in Fig. 5(d), the skin wounds of rats after 22 hours of infection are red, and purulent discharge is slightly visible. After 44 hours, it was clear that pus had formed at the edge of the rat's skin wound, and pus formation was the standard for infection, which is a pathological change that occurs when the broken wound or tissue is infected by germs.[43,44] Measurement of pH shows that the pH of the wound is about 7.0 at the time of formation, and the pH of the vulnus infection increases to a weak alkalinity (pH of about 8.5) after 22 hours. As shown in Fig. 5(e), the pH value increases from neutral to weakly alkaline compared to uninfected rats. Damage causes the underlying tissue to be exposed and changes the acidic environment in the area (the normal pH of the skin surface is acidic), but during wound infection, due to the multiplier and metabolism of bacteria, as well as the action of the animal's immune system, the pH of the wound reaches an alkaline state.[45,46] This is why pH is the main parameter for detecting wound conditions. Therefore, in this study, we used biomaterials to prepare a flexible wearable pH biometer for wound detection. We believe that with further sensors, this device can achieve real-time monitoring of wounds.

Conclusions

In this study, we prepared a wearable flexible pH biometer using the photosensitive protein bR to monitor the pH of wound infection. This biomaterial-based electrode is not only simple to prepare but also has good photoelectric properties and fast response. We perform performance analysis on pH biometers using photovoltage and compare them with commercial pH biometers. It was also demonstrated that a flexible pH biometer based on the photosensitive protein bR could accurately detect the pH of a wound infection. In addition, this photosensitive biomolecular material not only has a simple structure, fast response speed, and strong adaptability to the external environment, but also has many potential application values in the research and development and utilization of new photofunctional molecular materials.

Conflicts of interest

The authors declare no conflict of interest.

Acknowledgements

This study was supported by the National Key Research and Development Program of China (2022YFB3205600, 2021YFB3201200), National Natural Science Foundation of China (52372174, T2125003, 61875015), Carbon Neutrality Research Institute Fund (CNIF20230204), and the Fundamental Research Funds for the Central Universities (E3E46804).

References

1 M. Falcone, B. De Angelis, F. Pea, A. Scalise, S. Stefani, R. Tasinato, O. Zanetti and L. Dalla Paola, *J. Global Antimicrob. Resist.*, 2021, **26**, 140–147.
2 A. R. Siddiqui and J. M. Bernstein, *Clin. Dermatol.*, 2010, **28**, 519–526.
3 G. Xu, Y. Lu, C. Cheng, X. Li, J. Xu, Z. Liu, J. Liu, G. Liu, Z. Shi, Z. Chen, F. Zhang, Y. Jia, D. Xu, W. Yuan, Z. Cui, S. S. Low and Q. Liu, *Adv. Funct. Mater.*, 2021, **31**, 2100852.
4 B. P. Simmons, *Infect. Control Hosp. Epidemiol.*, 1982, **3**, 188–196.
5 L. A. Schneider, A. Korber, S. Grabbe and J. Dissemond, *Arch. Dermatol. Res.*, 2007, **298**, 413–420.
6 K. Huo, J. Zhang, T. Lin, Y. Zhang, Y. Liu and X. Liu, *Dyes Pigm.*, 2023, **219**, 111574.
7 S. Ono, R. Imai, Y. Ida, D. Shibata, T. Komiya and H. Matsumura, *Burns*, 2015, **41**, 820–824.
8 N. Jommanee, C. Chanthad and K. Manokruang, *Carbohydr. Polym.*, 2018, **198**, 486–494.
9 N. Pan, J. Qin, P. Feng, Z. Li and B. Song, *J. Mater. Chem. B*, 2019, **7**, 2626–2633.
10 A. Tamayol, M. Akbari, Y. Zilberman, M. Comotto, E. Lesha, L. Serex, S. Bagherifard, Y. Chen, G. Fu, S. K. Ameri, W. Ruan, E. L. Miller, M. R. Dokmeci, S. Sonkusale and A. Khademhosseini, *Adv. Healthcare Mater.*, 2016, **5**, 711–719.
11 K. Kiti, C. Thanomsilp and O. Suwantong, *Microchem. J.*, 2022, **177**, 107277.
12 J. Li, X. Zuo, H. Liu, Y. Xie and Y. Huang, *J. Iran. Chem. Soc.*, 2021, **18**, 2231–2239.
13 M. He, F. Ou, Y. Wu, X. Sun, X. Chen, H. Li, D. Sun and L. Zhang, *Mater. Des.*, 2020, **194**, 108913.
14 R. Rahimi, M. Ochoa, A. Tamayol, S. Khalili, A. Khademhosseini and B. Ziaie, *ACS Appl. Mater. Interfaces*, 2017, **9**, 9015–9023.
15 A. Pusta, M. Tertiş, C. Cristea and S. Mirel, *Biosensors*, 2022, **12**, 1.
16 S. Poëa-Guyon, H. Pasquier, F. Mérola, N. Morel and M. Erard, *Anal. Bioanal. Chem.*, 2013, **405**, 3983–3987.
17 P. Anees, K. V. Sudheesh, P. Jayamurthy, A. R. Chandrika, R. V. Omkumar and A. Ajayaghosh, *Chem. Sci.*, 2016, **7**, 6808–6814.

 This journal is © The Royal Society of Chemistry 2024

Published on 15 January 2024. Downloaded by Beijing Institute of Nanoenergy and Nanosystems CAS on 1/22/2024 11:26:07 AM.

18 S. Rao, Z. Guo, D. Liang, D. Chen, Y. Wei and Y. Xiang, *Phys. Chem. Chem. Phys.*, 2013, **15**, 15821–15824.
19 P. P. Kanekar, S. O. Kulkarni, C. V. Jagtap, V. S. Kadam and H. M. Pathan, *Sol. Energy*, 2020, **212**, 326–331.
20 A. E. Blaurock and W. Stoeckenius, *Nat. New Biol.*, 1971, **233**, 152–155.
21 H. W. Trissl and M. Montal, *Nature*, 1977, **266**, 655–657.
22 D. Oesterhelt and W. Stoeckenius, *Methods Enzymol.*, 1974, **31**, 667–678.
23 Q. Li, Y. T. Zhu, I. A. Kinloch and A. H. Windle, *J. Phys. Chem. B*, 2006, **110**, 13926–13930.
24 M. Katragadda, J. L. Alderfer and P. L. Yeagle, *Biochim. Biophys. Acta, Biomembr.*, 2000, **1466**, 1–6.
25 F. Hucho, *Angew. Chem., Int. Ed.*, 1998, **37**, 1518–1519.
26 L. Y. Jan, *Vision Res.*, 1975, **15**, 1081–1086.
27 J. K. Lanyi, *FEBS Lett.*, 1984, **175**, 337–342.
28 Y. Lv, N. Yang, S. Li, S. Lu and Y. Xiang, *Nano Energy*, 2019, **66**, 104129.
29 N. Hampp, *Chem. Rev.*, 2000, **100**, 1755–1776.
30 N. A. Hampp, *Appl. Microbiol. Biotechnol.*, 2000, **53**, 633–639.
31 Z. Ablonczy, V. H. Ha and E. Papp, *Biophys. Chem.*, 1998, **71**, 235–243.
32 M. Kono, S. Misra and T. G. Ebrey, *FEBS Lett.*, 1993, **331**, 31–34.
33 G. Nagel, B. Kelety, B. Möckel, G. Büldt and E. Bamberg, *Biophys. J.*, 1998, **74**, 403–412.
34 T. Miyasaka, K. Koyama and I. J. S. Itoh, *Science*, 1992, **255**, 342–344.
35 K. H. Zou, K. Tuncali and S. G. Silverman, *Radiology*, 2003, **227**, 617–628.
36 X. Zhang, Z. Li, T. Zhou, Q. Zhou, Z. Zeng, X. Xu and Y. Hu, *Talanta*, 2016, **150**, 184–189.
37 F. Shi, D. Shang and Z. Wang, *New J. Chem.*, 2019, **43**, 13398–13407.
38 B. Kuswandi, N. P. N. Asih, D. K. Pratoko, N. Kristiningrum and M. Moradi, *Packag. Technol. Sci.*, 2020, **33**, 321–332.
39 J. Gong, M. G. Tanner, S. Venkateswaran, J. M. Stone, Y. Zhang and M. Bradley, *Anal. Chim. Acta*, 2020, **1134**, 136–143.
40 T. Siripongpreda, B. Somchob, N. Rodthongkum and V. P. Hoven, *Carbohydr. Polym.*, 2021, **256**, 117506.
41 N. S. Alharbi, J. M. Khaled, S. Kadaikunnan, A. S. Alobaidi, A. H. Sharafaddin, S. A. Alyahya, T. N. Almanaa, M. A. Alsughayier and M. R. Shehu, *Saudi J. Biol. Sci.*, 2019, **26**, 1557–1562.
42 S. Liang, Q. Dang, C. Liu, Y. Zhang, Y. Wang, W. Zhu, G. Chang, H. Sun, D. Cha and B. Fan, *Carbohydr. Polym.*, 2018, **195**, 275–287.
43 N. K. Jain, D. E. Larson, K. W. Schroeder, D. D. Burton, K. P. Cannon, R. L. Thompson and E. P. DiMagno, *Ann. Intern. Med.*, 1987, **107**, 824–828.
44 M. Malone and G. Schultz, *Br. J. Dermatol.*, 2022, **187**, 159–166.
45 S. Li, Y. Zhang, H. Jin, H. Gao, S. Liu, W. Shi, W. Sun, Y. Liu and H. Zhang, *J. Colloid Interface Sci.*, 2023, **651**, 319–333.
46 Z. Zhang, R. Su, F. Han, Z. Zheng, Y. Liu, X. Zhou, Q. Li, X. Zhai, J. Wu, X. Pan, H. Pan, P. Guo, Z. Li, Z. Liu and X. Zhao, *RSC Adv.*, 2022, **12**, 3243–3252.